Solid State Sciences 100 (2020) 106064

Contents lists available at ScienceDirect

Solid State Sciences

journal homepage: http://www.elsevier.com/locate/ssscie

# Synthesis, crystal structure, optical absorption study, and electronic structure of $Cs_3FeCl_5$

Subhendu Jana [a], Gopabandhu Panigrahi [a], S. Narayanswamy [b], Mohd Ishtiyak [a], Manajit Das [a], Pinaki P. Bhattacharjee [b], Manish K. Niranjan [c], Jai Prakash [a,*]

[a] Department of Chemistry, Indian Institute of Technology Hyderabad, Kandi, Sangareddy, Telangana, 502285, India
[b] Department of Materials Science & Metallurgical Engineering, Indian Institute of Technology Hyderabad, Kandi, Sangareddy, Telangana, 502285, India
[c] Department of Physics, Indian Institute of Technology Hyderabad, Kandi, Sangareddy, Telangana, 502285, India

ARTICLE INFO

*Keywords:*
Molten-flux method
Crystal structure
Optical absorption
Band gap
Electronic structure

ABSTRACT

The single crystals of $Cs_3FeCl_5$ were synthesized at 973 K using the sealed tube solid-state molten flux method using CsCl as a reactive flux. The polycrystalline sample of $Cs_3FeCl_5$ was obtained by the stoichiometric reaction of CsCl and $FeCl_2$ powders at 823 K by the sealed tube solid-state method. The crystal structure of $Cs_3FeCl_5$ was determined by single-crystal X-ray diffraction study at 298 (2) K. This ternary halide crystallizes in the body-centered tetragonal crystal system in *I4/mcm* space group with cell constants of $a = b = 9.279$ (1) Å and $c = 14.824$ (3) Å with four formula units per cell. The asymmetric unit of $Cs_3FeCl_5$ contains five crystallographically independent atomic sites: Cs1 (site symmetry: *m*.2 *m*), Cs2 (422), Fe1 ($\bar{4}2\,m$), Cl1 (..*m*), and Cl2 (4/*m*..). Each Fe atom in $Cs_3FeCl_5$ structure is bonded to four Cl1 atoms in a slightly distorted tetrahedral fashion to form isolated $FeCl_4^{2-}$ units. These $FeCl_4^{2-}$ units are separated by the $Cs^+$ cations and infinite [CsCl] linear chains. Charge balance in this closed-shell compound can be achieved by $3 \times Cs^+$, $1 \times Fe^{2+}$, and $5 \times Cl^-$. Bond valence sum (BVS) calculation also supports this assignment of formal oxidation states of elements in $Cs_3FeCl_5$ structure. The electronic structure calculation for $Cs_3FeCl_5$ performed within a density functional theoretical framework predicts a band gap of 3.5 eV, which is in good agreement with the experimental band gap of 3.71 (2) eV, that was estimated from the UV–vis absorption edge study of polycrystalline $Cs_3FeCl_5$.

## 1. Introduction

During the last few decades, a variety of new metal halides have been synthesized to study the structure-physical property relationships to fine-tune their physical properties for various applications such as solar cell, light-emitting devices, and magnetic properties [1–3], etc. Among these compounds, metal halides with perovskite structure like $CH_3NH_3PbX_3$ (X = Cl, Br, I) [4], $CsMX_3$ (M = Pb, Sn) [4], and $Cs_2MX_4$ [4] are extensively studied for solar cell applications. Furthermore, ternary halides like $CsPbX_3$ (X = Cl, Br, or I) have been well studied for their light-emitting device applications [2]. Magnetic properties of alkali and transition metal-based ternary halides have been previously reported in the compounds like $KFeCl_3$ [5], $Cs_2CoCl_4$ [3], $Cs_3CoCl_5$ [6,7], $Cs_3MnCl_5$ [8], and $Cs_3NiCl_5$ [9].

The compounds having empirical molecular formula $A_3MX_5$ (A = $NH_4$, K, Rb, Cs, Tl, M = transition metal, and X = Cl, Br, I) mainly crystallize in three different structure types [10]. All these structure types contain the isolated $MX_4^{2-}$ tetrahedral units [10]. The most common structure type of this $A_3MX_5$ family of compounds is tetragonal $Cs_3CoCl_5$ structure type (space group: *I4/mcm*) [11]. Compounds like $Cs_3MI_5$ (M = Mn, Cd, Zn) [10], $Cs_3NiCl_5$ [12], $Cs_3FeBr_5$ [13], $Tl_3FeCl_5$ [13], $Cs_3MnBr_5$ [13], $Tl_3CoCl_5$ [13], $Cs_3ZnBr_5$ [14], $Cs_3CdBr_5$ [15], and $Cs_3CoBr_5$ [16] crystallize in this $Cs_3CoCl_5$ structure type. The second structure type of $A_3MX_5$ family is $(NH_4)_3ZnCl_5$ structure type [17], which crystallizes in the orthorhombic *Pnma* space group. Examples of compounds that adopts $(NH_4)_3ZnCl_5$ structure type are $Cs_3ZnI_5$ [18], $Rb_3ZnBr_5$ [19], $Cs_3CoI_5$ [18], $Cs_3HgCl_5$ [20], $Cs_3HgBr_5$ [21], $(NH_4)_3CoCl_5$ [13], and $(NH_4)_3FeCl_5$ [13]. The third structure type known in this family is $Cs_3HgI_5$ structure type [22] with orthorhombic space group *Pbca*. Although the basic building blocks ($MX_4^{2-}$ units) of all these compounds are same but the relative sizes of cations and $X^-$ anions plays an important role in stabilization of one of the three known structure types. For instance, replacement of smaller $Cl^-$ anion with bigger $I^-$ anion in $Cs_3CoCl_5$ structure leads to lowering of symmetry

* Corresponding author.
*E-mail address:* jaiprakash@iith.ac.in (J. Prakash).

https://doi.org/10.1016/j.solidstatesciences.2019.106064
Received 19 September 2019; Received in revised form 18 October 2019; Accepted 7 November 2019
Available online 15 November 2019

form tetragonal to orthorhombic. In general, $A_3MX_5$ structures with large cation or anion favors the orthorhombic structures.

There are four compounds known in the Cs–Fe–Cl ternary phase diagram: $CsFeCl_3$ [23], $CsFeCl_4$ [24], $Cs_3FeCl_5$ [25], and $Cs_3Fe_2Cl_9$ [26]. The crystal structures of $CsFeCl_3$ [23], $CsFeCl_4$ [24], and $Cs_3Fe_2Cl_9$ [26] have been reported previously. There are several reports on the synthesis of $Cs_3FeCl_5$, but the crystal structure of $Cs_3FeCl_5$ is not determined in the past. Seifert et al. have synthesized this compound earlier and have only reported the cell constants of $Cs_3FeCl_5$ structure using the powder X-ray diffraction data. In this article, we are presenting the crystal structure of $Cs_3FeCl_5$ structure using the single-crystal X-ray diffraction study for the first time. We have also optimized the reaction conditions to produce an almost monophasic polycrystalline sample of $Cs_3FeCl_5$ in one step. The optical absorption study and electronic structure of $Cs_3FeCl_5$ are also presented in this article.

## 2. Experimental

### 2.1. Synthesis

The following reactants were used as received: cesium chloride (99.9%, SRL), iron powder (99.98%, Alfa Aesar), sulfur powder (>99.5%, Sigma Aldrich), phosphorus powder (99%, Alfa Aesar), and ferrous chloride (99.5%, Alfa Aesar). These reactants are air and moisture sensitive, and hence, all of the chemical manipulations were performed inside the Ar-filled dry glove box.

$P_2S_5$ was synthesized by a stoichiometric reaction of red phosphorous and sulfur powder in a sealed evacuated (*ca.* $10^{-4}$ Torr) carbon-coated fused silica tube. The reaction mixture was heated to 733 K in 30 h, and annealed for 24 h and then cooled to room temperature in 10 h. A very light yellow colored product was obtained that was homogenized inside the Ar-filled dry glove box using an agate mortar and pestle.

#### 2.1.1. Synthesis of single crystals of $Cs_3FeCl_5$

Transparent colorless block shaped crystals of $Cs_3FeCl_5$ were obtained as a byproduct of a reaction that was aimed for the synthesis of a quaternary $Cs_2FeP_2S_6$ compound. In an attempt to synthesize $Cs_2FeP_2S_6$, an excess amount of CsCl (361.7 mg, 2.148 mmol) along with Fe (40 mg, 0.7162 mmol), $P_2S_5$ (79.6 mg, 0.3581 mmol), and S (34.4 mg, 1.0745 mmol) were loaded in a carbon coated fused silica tube in an Ar-filled glove box. The flame-sealed evacuated tube (*ca.* $10^{-4}$ Torr) was first heated to 973 K in 15 h and annealed for 6 h. The tube was then slowly cooled to 673 K in 75 h and, annealed there for 24 h, followed by further cooling to 373 K in 60 h before switching off the furnace. The reaction product was consisting of small transparent white crystals along with a yellow powder. The elemental compositions of these transparent crystals were estimated by energy dispersive spectroscopy (EDS) studies using octane elite (EDAX Inc., USA) spectrometer that was attached to the field-emission scanning electron microscope (FE-SEM) (Make: JEOL, Japan; Model: JSM 7800F). The EDS data were collected with an accelerating voltage of 15–20 kV. The EDS analysis of the crystals was performed by choosing multiple random points on the various selected crystals. The average composition of the crystal was found to be in the ratio of ≈3:1:5 with respect to cesium, iron, and chlorine, respectively without any other impurities (Fig. 1a).

#### 2.1.2. Synthesis of polycrystalline $Cs_3FeCl_5$

Synthesis of polycrystalline $Cs_3FeCl_5$ was carried out using the sealed tube solid-state method. A stoichiometric amount of CsCl (399.7 mg, 2.37 mmol) and $FeCl_2$ (100.3 mg, 0.79 mmol) were loaded inside a carbon-coated fused silica tube having 10 mm inner diameter and 12 mm outer diameter in an Argon filled glove box. These reactants were dried in an oven before the reaction to remove any undesired moisture. The fused silica tube containing the reaction mixture was first evacuated (*ca.* $10^{-4}$ Torr) and sealed using a flame torch. The sealed ampoule was then placed inside a programmable muffle furnace, and the temperature was slowly ramped up to 823 K temperature with a heating rate of 9 K/h. The reaction mixture was annealed at 823 K for 36 h before switching the furnace off. A homogeneous looking ingot was obtained after the reaction that was ground into a fine powder. The Powder X-ray diffraction data of this white polycrystalline product was collected for phase identification.

### 2.2. Single crystal X-ray diffraction study of $Cs_3FeCl_5$

Single-crystal X-ray diffraction data of $Cs_3FeCl_5$ crystal were collected at 298 (2) K on a Rigaku Supernova X-Calibur equipped with Eos CCD detector with a graphite monochromatic Mo-$K\alpha$ radiation ($\lambda = 0.71073$ Å). The quality of single crystals was judged from reflections collected for the unit cell determination. A suitable sized single crystal was picked under Paratone-N oil and was mounted on a KM4/Xcalibur Goniometer. The crystal-to-detector distance was 45 mm, and the exposure time was 20 s/frame. Collection of intensity data, cell refinement, and data reduction were performed using *CrysAlis$^{pro}$* as a series of 0.6° in $\omega$ scans [27]. The absorptions corrections were performed by SCALE3 ABSPACK multi-scan method [28].

The SHELX-14 suite of programs was used to solve the crystal structure of $Cs_3FeCl_5$. The XPREP program recommended body (I) centered tetragonal cell. Value of mean $|E^2 - 1|$ (0.88) suggested a centrosymmetric space group. XPREP program offered three space groups on the basis of systematic absences: *I4/mcm* (centrosymmetric), *I4cm* (non-centrosymmetric) and $I\bar{4}c2$ (non-centrosymmetric). We used most symmetric space group *I4/mcm* (no 140) among these three space groups to solve the crystal structure using the direct method. The refinement of the crystal structure model was carried out using the

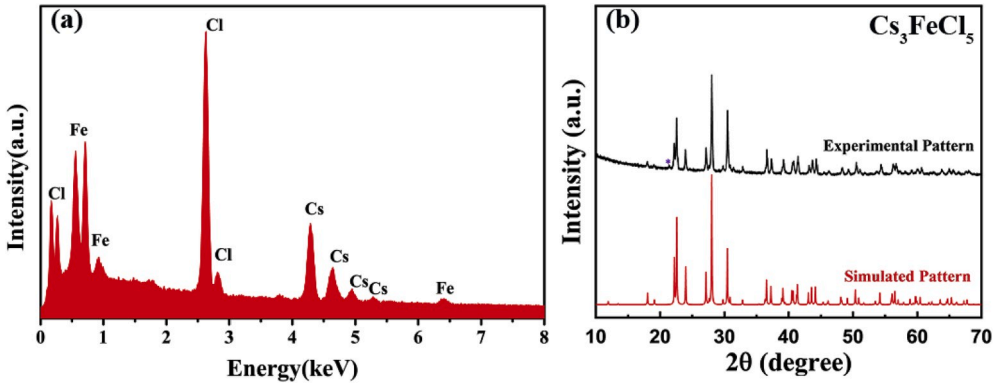


**Fig. 1.** **(a)** The EDS spectrum of one of the $Cs_3FeCl_5$ crystal and **(b)** PXRD pattern of polycrystalline $Cs_3FeCl_5$. Reflection corresponding to the minor secondary phase CsCl is shown by * symbol.

SHELXTL program package [29] which used full-matrix least-squares on $F^2$ method. Scale factors, weight correction, atomic positions with anisotropic displacement parameters, and extinction parameter were refined. As the value of the extinction parameter was found to be nearly zero, the refinement of the extinction parameter was excluded from the final cycles of the structure refinement. The solved structure model was examined using the ADDSYM program [30] of PLATON [30] that did not detect any missing symmetry. Finally, the STRUCTURE TIDY program [30] was used to standardize the atomic positions in $Cs_3FeCl_5$ structure. Further crystallographic and structural details are presented in Tables 1–3.

### 2.3. Powder X-ray diffraction study (PXRD)

The PXRD data of a homogenized powdered sample of $Cs_3FeCl_5$ was carried out at room temperature using a PAN analytical empyrean diffractometer with Cu-*K*α radiation (λ = 1.5406 Å) source. The PXRD data was recorded over a 2θ range of 10°–70° using a θ-2θ geometry. The phase analysis of the PXRD data was performed using the *Match!* Version 2 software.

### 2.4. Solid-state ultraviolet–visible (UV–vis) spectroscopy

The optical band gap study of $Cs_3FeCl_5$ was carried out at room temperature (298 (2) K). Polycrystalline $Cs_3FeCl_5$ sample was properly ground into a fine powder inside an Ar-filled glove box, and then mixed with dried $BaSO_4$ that acts as a standard reference for the UV–vis absorption study. Shimadzu UV-3600 instrument was used to collect the data in diffuse reflectance mode vs. wavelength over the wavelength range of 800 nm (1.55 eV) to 200 nm (6.2 eV). Kubelka–Munk equation $\alpha/S = (1 - R)^2/2R$ was used to convert the reflectance data into absorption data. Here $\alpha$, $S$, and R are the absorption coefficient, scattering coefficient, and reflectance, respectively [31]. The absorption vs. energy plot was used to estimate the band gap by absorption edge study.

### 2.5. Electronic structure calculation methodology

The first-principles calculations are performed within the framework of density functional theory (DFT) [32] using the projected augmented wave (PAW) potentials [33] as implemented in the VASP Package [34,35]. The Perdew-Burke-Ernzerhoff (PBE) [36] form of generalized gradient approximation (GGA) is used to approximate the exchange-correlation functional. The Kohn-Sham wavefunctions are expanded in plane-wave basis set with a kinetic energy cutoff of 320 eV and higher. The Brillouin zone is sampled using $8 \times 8 \times 6$ Monkhorst-Pack *k*-point mesh. The lattice constants and the atomic positions in the unit cell are relaxed until the strongest force becomes less than $10^{-2}$ eV/Å. Self-consistency in calculations is achieved by allowing the total energies to converge up to $10^{-6}$ eV/cell.

**Table 1**
**Crystallographic data for $Cs_3FeCl_5$[a].**

| | $Cs_3FeCl_5$ |
|---|---|
| Space group | $D_{4h}^{18}$–*I*4/*mcm* |
| *a* (Å) | 9.2794 (13) |
| *b* (Å) | 9.2794 (13) |
| *c* (Å) | 14.824 (3) |
| *V* (Å$^3$) | 1276.5 (4) |
| *Z* | 4 |
| *ρ* (g cm$^{-3}$) | 3.288 |
| *μ* (mm$^{-1}$) | 10.60 |
| *R*(*F*)[b] | 0.023 |
| $R_w$ ($F_o^2$)[c] | 0.055 |

[a] λ = 0.71073 Å, *T* = 298 (2) K.
[b] $R(F) = \Sigma\ ||F_o|-|F_c||/\Sigma|F_o|$ for $F_o^2 > 2\sigma(F_o^2)$.
[c] $R_w(F_o^2) = \{\Sigma\ [w\ (F_o^2 - F_c^2)^2]/\Sigma wF_o^4\}^{1/2}$. For $F_o^2 < 0$, $w = 1/[\sigma^2\ (F_o^2) + (0.0264P)^2]$; where $P = (F_o^2 + 2F_c^2)/3$.

**Table 2**
Fractional Atomic Coordinates and isotropic or equivalent isotropic displacement parameters (Å$^2$)[a] for $Cs_3FeCl_5$ structure.

| Atoms | Wyckoff Position | *x* | *y* | *z* | $U_{iso}/U_{eq}$[a] |
|---|---|---|---|---|---|
| Cs1 | 8*h* | 0.16555 (2) | 0.16555 (2) | 0.0000 | 0.03093 (14) |
| Cs2 | 4*a* | 0.0000 | 0.0000 | 0.2500 | 0.04322 (18) |
| Fe1 | 4*b* | 0.0000 | 0.5000 | 0.2500 | 0.0280 (2) |
| Cl1 | 16*l* | 0.64042 (9) | 0.14042 (9) | 0.15623 (9) | 0.0446 (3) |
| Cl2 | 4*c* | 0.0000 | 0.0000 | 0.0000 | 0.0373 (4) |

[a] $U_{iso}/U_{eq}$ is the one third value of the trace of orthogonalized $U_{ij}$ tensor.

**Table 3**
Selected interatomic lengths (Å) and angles (deg.) for $Cs_3FeCl_5$.

| Atom pair and bond angles | Distances (Å) and angles (deg.) |
|---|---|
| Cs1–Cl1 | 3.4419 (12) × 2 |
| | 3.6715 (12) × 4 |
| Cs1–Cl2 | 3.4629 (5) × 2 |
| Cs2–Cl1 | 3.8423 (8) × 8 |
| Cs2–Cl2 | 3.7061 (2) × 2 |
| Fe1–Cl1 | 2.3083 (11) × 4 |
| Fe1· ·Fe1 | 6.562 (1) |
| Cs1· ·Cs1 | 4.3452 (9) |
| Cs2· ·Cs2 | 7.412 (1) |
| Cs1· ·Cs2 | 5.072 (1) |
| Cs1· ·Fe1 | 4.2959 (7) |
| Cs2· ·Fe1 | 4.640 (1) |
| Cl1–Fe1–Cl1 | 111.26 (3) × 4 |
| Cl1–Fe1–Cl1 | 105.94 (7) × 2 |

## 3. Results and discussion

### 3.1. Syntheses and crystal structure

The transparent colorless block shaped crystals of $Cs_3FeCl_5$ were first obtained as a byproduct in a reaction of Fe, $P_2S_5$, and S powders in excess of CsCl flux at 973 K using the high-temperature sealed tube method. The experimental PXRD pattern of $Cs_3FeCl_5$ is in an excellent agreement with the simulated PXRD pattern that was obtained by the single crystal X-ray study (Fig. 1b). A tiny amount of CsCl was also detected as a minor secondary phase along with the major tetragonal $Cs_3FeCl_5$ phase.

*Crystal structure description of $Cs_3FeCl_5$.* The crystal structure of $Cs_3FeCl_5$ adopts $Cs_3CoCl_5$ structure type [11]. It crystallizes with four formula units in the space group *I*4/*mcm* of the tetragonal system with unit cell lengths of $a = b = 9.279$ (1) Å and $c = 14.824$ (3) Å. The unit cell constants of $Cs_3FeCl_5$ are slightly larger than the isotopic $Cs_3CoCl_5$ structure ($a = b = 9.232$ (1) Å and $c = 14.554$ (1) Å) due to smaller ionic size of $Co^{2+}$ (0.58 Å) as compared to $Fe^{2+}$ ion (0.63 Å) [11]. The asymmetric unit of the structure is composed of five crystallographically independent sites: Cs1 (site symmetry: *m*.2*m*), Cs2 (422), Fe1 ($\bar{4}2m$), Cl1 (..*m*), and Cl2 (4/*m*..). The crystal structure of this ternary halide is of a pseudo-zero-dimensional type with isolated $[FeCl_4^{2-}]$ units that are separated by $Cs^+$ cations and infinite [CsCl] linear chains (Fig. 2). Each Fe atom is coordinated to four Cl1 atoms forming a distorted tetrahedral geometry as evident from Fig. 2. The coordination number of Cs1 atom is eight. Each Cs1 atom is surrounded by six Cl1 and two Cl2 atoms that form a distorted bicapped trigonal prism-like geometry, as shown in Fig. 3a. In contrast to Cs1, the coordination number of Cs2 atoms is ten: there are eight Cl1 and two Cl2 atoms around each Cs2 atom, forming a distorted bicapped square antiprism like geometry (Fig. 3b). The Cs2

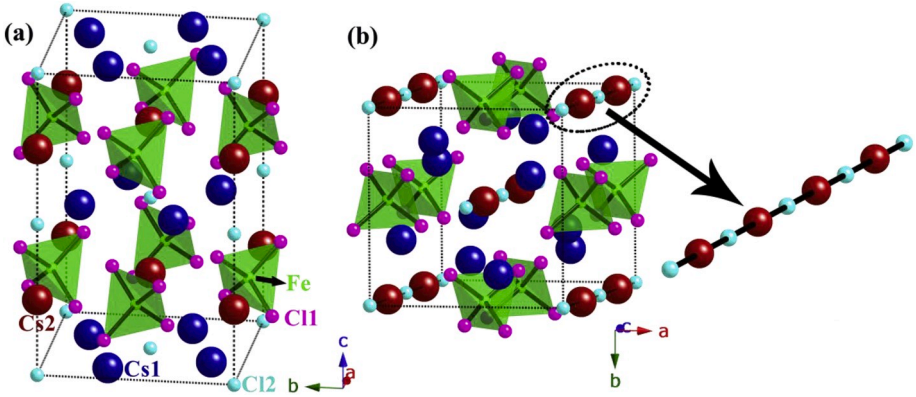


**Fig. 2.** The unit cell structure of the tetragonal $Cs_3FeCl_5$ (space group: I 4/*mcm*) approximately along **(a)** [100] and **(b)** [001] directions. The linear chain that is made up of Cs2 and Cl2 atoms is shown on the right side of Fig. 2b. The Cs1, Cs2, Fe1, Cl1, and Cl2 atoms are shown in royal blue, cherry red, green, pink, and sky blue colors. (For interpretation of the references to color in this figure legend, the reader is referred to the Web version of this article.)

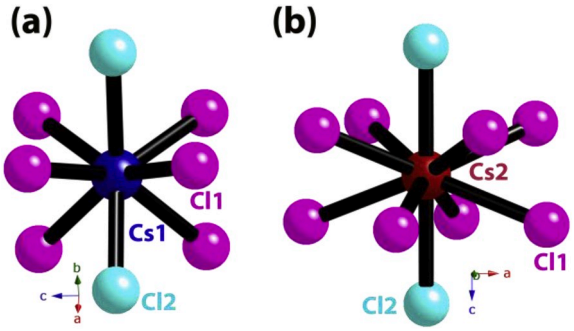


**Fig. 3.** Local coordination environments around **(a)** Cs1 and **(b)** Cs2 atoms in $Cs_3FeCl_5$ structure.

and Cl2 atoms are forming the linear infinite chains that are running along the *c*-direction as shown in Fig. 2b. Each $FeCl_4^{2-}$ tetrahedral unit contains four equal Fe–Cl bond distances of 2.3081 (11) Å which are shorter than the sum of the ionic radii of $Fe^{2+}$ and $Cl^-$ ions (2.44 Å) [37]. This observation suggests a covalent bonding between Fe and Cl atoms. The $Fe^{2+}$–$Cl^-$ bond distances in $Cs_3FeCl_5$ structure are in good agreement with those found in the metal complexes such as $([C_5H_5S_2]_2[FeCl_4]$ (2.289 (5)−2.335 (5) Å) [38] and $[N(CH_3)_4]_2[FeCl_4]$ (2.289 (2)−2.296 (2) Å) [39]. The tetrahedral coordination environment of iron atoms in the $Cs_3FeCl_5$ structure suggests the high spin state of $Fe^{2+}$ ($3d^6$) with $e^3t_2^3$ electronic configuration since $Cl^-$ is a weak field ligand.

The two different types of Cl1–Fe–Cl1 bond angles of 111.26 (3)° ( × 4) and 105.95 (7)° ( × 2) in $FeCl_4^{2-}$ units of $Cs_3FeCl_5$ structure suggest that these tetrahedral are slightly distorted. The Cs1–Cl bond distances vary from 3.4419 (12) Å to 3.6715 (12) Å with an average of 3.5619 (1) Å. These distances are comparable to corresponding $Cs^+$–Cl distances in related compounds with similar coordination geometry e.g., $Cs_3MnCl_5$ (3.41 (1) to 3.66 (1) Å) [40], $Cs_3CoCl_5$ (3.424 (1) to 3.642 (1) Å) [11], and $Cs_3NiCl_5$ (3.431 (2) to 3.627 (2) Å) [12]. The Cs2–Cl distances (3.7061 (2) to 3.8423 (8) Å) are longer than the two different Cs1–Cl bond distances as expected due to higher coordination number. The average Cs2–Cl bond distance is 3.815 (1) Å.

The Cs2–Cl distances found in $Cs_3FeCl_5$ structure are comparable to corresponding distances in related structures e.g., $Cs_3MnCl_5$ (3.74 (1) to 3.82 (1) Å) [40], $Cs_3NiCl_5$ (3.638 (1) to 3.823 (1) Å) [12], and $Cs_3CoCl_5$ (3.638 (1) to 3.813 (1) Å) [11].

$Cs_3FeCl_5$ structure does not show any homoatomic bonding and hence can be easily charge-balanced based on the Zintl formalism with $3 \times Cs^+$, $1 \times Fe^{2+}$, and $5 \times Cl^-$. Furthermore, bond valence sum (BVS) calculation [41,42] for $Cs_3FeCl_5$ structure also suggests the same assignment of formal charges as discussed above, i.e. $(Cs^+)_3(Fe^{2+})(Cl^-)_5$. However, the BVS value of Cs2 atom is slightly lower than the expected value of one (Table 4). The Cl2 atom is expected to show a smaller BVS value than the Cl1 as the coordination number for Cl2 (10) is greater than Cl1 (8) atom. Also, the lower BVS value of Cs2 than Cs1 can also be interpreted as a slight underbonding of Cs2 cation with chloride ion.

### 3.2. Optical band gap study of $Cs_3FeCl_5$

An absorption spectrum of polycrystalline $Cs_3FeCl_5$ was collected in the wavelength region starting from 800 nm (1.55 eV) to 200 nm (6.2 eV) to estimate the band gap of this compound. The variation of absorption ($\alpha/S$) as a function of energy (eV) is shown in Fig. 4. It is evident from this figure that $Cs_3FeCl_5$ mainly absorbs in the UV region of the electromagnetic spectrum. The absorption edge study of this plot suggests a band gap of 3.71 (2) eV (Fig. 4). Hence, $Cs_3FeCl_5$ could be classified as a wide band gap insulator.

### 3.3. Electronic structure of $Cs_3FeCl_5$

Next, we study the atomic and electronic structure of $Cs_3FeCl_5$. The computed lattice parameters and fractional atomic coordinates are shown in Table 5. As evident, the theoretical estimates of the lattice constants and fractional atomic coordinates are in good agreement (<1.6%) with the corresponding experimental values. The computed unit cell volume is found to be smaller by ~3.5% than the experimental volume. The total and projected density of electronic states of $Cs_3FeCl_5$ are shown in Fig. 5. The valence band (VB) extends from ~ − 6 eV to 0 eV. The states within ~1 eV below the valence band maximum (VBM, 0 eV) are contributed by 3*d* states of Fe atoms as can be seen in Fig. 5b. A small contribution of Cl-3*p* states at VBM can also be seen. In the energy range from −2 eV to −4 eV, the states are primarily contributed by Cl-3*p* orbitals. The hybridization between Cl-3*p* and Fe-3*d* orbitals in the ~ − 3 to ~ − 4.5 eV energy range of VB can be seen in Fig. 5. Further, a weak hybridization between Cl-3*p* and Fe-4*s* orbitals is also evident in energy

**Table 4**
Bond valence sums (BVS) for atoms in $Cs_3FeCl_5$.

| Site | BVS |
|---|---|
| Cs1 | 1.0401 |
| Cs2 | 0.6354 |
| Fe1 | 2.2177 |
| Cl1 | 1.0285 |
| Cl2 | 0.8194 |

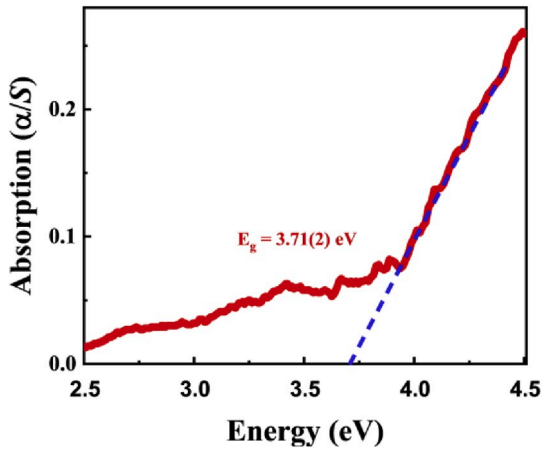


**Fig. 4.** Optical UV–vis absorption spectrum of polycrystalline $Cs_3FeCl_5$.

**Table 5**
The computed fractional coordinates of atoms at nonequivalent sites in tetragonal $Cs_3FeCl_5$. The calculated lattice constants (*a, b, c*) and volume (*V*) are $a = b = 9.1879$ Å, $c = 14.5952$ Å and $V = 1232.09$ Å$^3$ The experimental lattice constants and volume are $a = b = 9.2794$ (13) Å, $c = 14.824$ (3) Å and $V = 1276.45$ Å$^3$.

| Site | | *x* | *y* | *z* |
|---|---|---|---|---|
| Cl1 | **cal.** | 0.6371 | 0.1371 | 0.1578 |
| | **exp.** | 0.6404 | 0.1404 | 0.1562 |
| Cl2 | **cal.** | 0.0 | 0.0 | 0.0 |
| | **exp.** | 0.0 | 0.0 | 0.0 |
| Cs1 | **cal.** | 0.1649 | 0.6649 | 0.0 |
| | **exp.** | 0.1655 | 0.6655 | 0.0 |
| Cs2 | **cal.** | 0.0 | 0.0 | 0.25 |
| | **exp.** | 0.0 | 0.0 | 0.25 |
| Fe1 | **cal.** | 0.0 | 0.5 | 0.25 |
| | **exp.** | 0.0 | 0.5 | 0.25 |

range ~ −5.5 eV to ~ −6.0 eV. The states in the energy range from −8 to −9 eV are contributed by Cs-5*p* orbitals. The Cl-3*s* states contribute in the energy range from ~ −14 eV to −16 eV. The states at ~ −21.5 eV are comprised of Cs-5*s* orbitals. The conduction band (CB) is comprised of primarily by hybridized Cs-5*d* and Fe-3*d* states. As can be seen in Fig. 5, the computed bandgap is found to be ~3.5 eV, which is in good agreement with the experimental gap of ~3.7 eV. It may be noted that reasonable agreement of theoretical bandgap estimate with experimental bandgap may be a coincidence as DFT bandgap estimates are generally expected to be underestimated.

## 4. Conclusions

Single crystals of transition metal-based ternary halide, $Cs_3FeCl_5$, were grown inside a sealed carbon-coated fused silica tube at 973 K using the molten flux of CsCl that acted as a reactive flux. The polycrystalline phase of $Cs_3FeCl_5$ was also synthesized at 823 K by the sealed tube solid-state synthesis. The single-crystal study shows that $Cs_3FeCl_5$ crystallizes in the $Cs_3CoCl_5$ structure type in the tetragonal space group, *I*4/*mcm*. $Cs_3FeCl_5$ structure consists of five crystallographically independent sites: Cs1 (site symmetry: *m*.2*m*), Cs2 (422), Fe1 ($\bar{4}2m$), Cl1 (..*m*) and Cl2 (4/*m*..). The crystal structure of $Cs_3FeCl_5$ is made up of isolated tetrahedral units of $[FeCl_4^{2-}]$ that are separated by $Cs^+$ cations and infinite [CsCl] chains. The UV–vis absorption study confirms the insulating nature of $Cs_3FeCl_5$ with a band gap of 3.71 (2) eV. The electronic structure of $Cs_3FeCl_5$ obtained by the DFT study shows that the valence band is dominated by the Fe-3*d* and Cl-3*p* states. In particular, the states in the vicinity of VBM are comprised of Fe-3*d* orbitals. The DFT calculations also suggest insulating behavior with a theoretical band gap

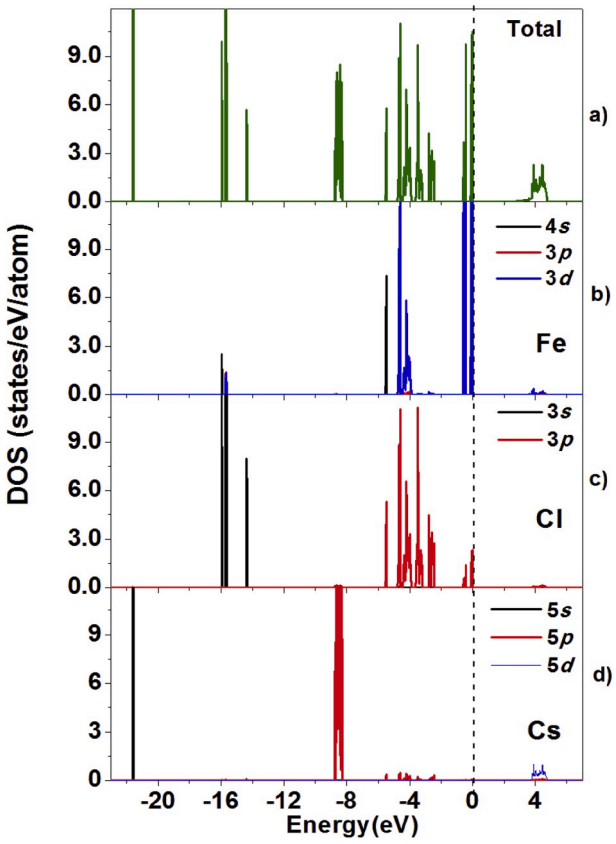


**Fig. 5. (a)** The total density of states of $Cs_3FeCl_5$. **(b)** The partial density of states (PDOS) projected onto Fe atom, **(c)** Cl atom, and **(d)** Cs atom. The valence band maximum is shown by the black dashed line.

of 3.5 eV which is in good agreement with the optical band gap of 3.71 (2) eV.

## Supporting information

Crystallographic data in CIF format for $Cs_3FeCl_5$ has been deposited with the Cambridge Crystallographic Data Centre as CCDC# 1953419. This data may be obtained free of charge by contacting CCDC at https://www.ccdc.cam.ac.uk/.

## Acknowledgments

JP thanks DST-SERB, Government of India for the financial support under early career research (ECR) award (Grant number: ECR/2017/000822) and IIT Hyderabad for seed grant and research facilities. SJ and GP thank MHRD, IIT Hyderabad for the research fellowships. MI thanks DST India for the research fellowship. The authors also gratefully acknowledge DST-FIST (SR/FST/ETI-421/2016) for the SEM-EDS facility used in this work.

## Appendix A. Supplementary data

Supplementary data to this article can be found online at https://doi.org/10.1016/j.solidstatesciences.2019.106064.

## References

[1] Q. Wang, N. Phung, D.D. Girolamo, P. Vivo, A. Abate, Enhancement in lifespan of halide perovskite solar cells, Energy Environ. Sci. 12 (2019) 865–886, https://doi.org/10.1039/C8EE02852D.
[2] Q. Zhang, M.M. Tavakoli, L. Gu, D. Zhang, L. Tang, Y. Gao, J. Guo, Y. Lin, S.-F. Leung, S. Poddar, Y. Fu, Z. Fan, Efficient metal halide perovskite light-emitting

diodes with significantly improved light extraction on nanophotonic substrates, Nat. Commun. 10 (2019) 1–9, https://doi.org/10.1038/s41467-019-08561-y.
[3] C.J. Mukherjee, R. Coldea, D.A. Tennant, M. Koza, M. Enderle, K. Habicht, P. Smeibidl, Z. Tylczynski, Field-induced quantum phase transition in the quasi 1D XY-like antiferromagnet $Cs_2CoCl_4$, J. Magn. Magn. Mater. 272–276 (2004) 920–921, https://doi.org/10.1016/j.jmmm.2003.12.1115.
[4] S.-T. Ha, R. Su, J. Xing, Q. Zhang, Q. Xiong, Metal halide perovskite nanomaterials: synthesis and applications, Chem. Sci. 8 (2017) 2522–2536, https://doi.org/10.1039/C6SC04474C.
[5] V. Petrouleas, Relaxation effects and evidence for one dimensional ordering in $KFeCl_3$ studied by Mössbauer spectroscopy, Solid State Commun. 15 (1974) 1097–1100, https://doi.org/10.1016/0038-1098(74)90540-7.
[6] R.H. Holm, F.A. Cotton, Magnetic investigations of spin-free cobaltous complexes. I. Tetrahalo cobalt(II) ions, J. Chem. Phys. 31 (1959) 788–792, https://doi.org/10.1063/1.1730463.
[7] T. Qu, X.-Y. Kuang, Y.-F. Li, R.-P. Chai, Theoretical investigations of the electronic and magnetic structures for the $[CoCl_4]^{2-}$ cluster in $Cs_3CoCl_5$ crystal, Chem. Phys. Lett. 504 (2011) 170–174, https://doi.org/10.1016/j.cplett.2010.12.079.
[8] J.C. Rivoal, B. Briat, J.P. Torre, Magneto-optical determination of magnetic ordering and magnetic structure of $Cs_3MnCl_5$ below 0.6 K, J. Appl. Phys. 53 (1982) 2713–2715, https://doi.org/10.1063/1.330941.
[9] R. Wojciechowska, J. Mulak, W. Trzebiatowski, Magnetic properties of $CsNiCl_3$ and $Cs_3NiCl_5$ in crystalline and fused states, Bulletin de l'Academie Polonaise Des Sciences, Ser. Des. Sci. Chim. 18 (1970) 127–132.
[10] R. Sjövall, C. Svensson, Crystal structures of four $Cs_3MI_5$ (M = Mn, Cd, Hg) phases and structural relationship among $Cs_3MI_5$ compounds, Z. für Kristallogr. - Cryst. Mater. 212 (1997) 732–741, https://doi.org/10.1524/zkri.1997.212.10.732.
[11] P.A. Reynolds, B.N. Figgis, A.H. White, An X-ray diffraction study of tricaesium tetrachlorocobaltate(II) chloride at 295 K, Acta Crystallogr. B 37 (1981) 508–513, https://doi.org/10.1107/S056774088100349X.
[12] M. Sassmannshausen, H.D. Lutz, Caesium nickel(II) trichloride, $CsNiCl_3$, and tricaesium nickel(II) pentachloride, $Cs_3NiCl_5$, Acta Crystallogr. C 54 (1998) 704–706, https://doi.org/10.1107/S0108270197019598.
[13] M. Amit, A. Horowitz (Zodkevitz, E. Ron, J. Makovsky, PREPARATION AND CRYSTAL STRUCTURES OF SOME COMPOUNDS OF THE $A_3BX_5$ TYPE (A = Cs, Tl, $NH_4$, B = Mn, Fe, Co, X = Cl, Br), Isr. J. Chem. 11 (1973) 749–764, https://doi.org/10.1002/ijch.197300074.
[14] A.S. Kanishcheva, I.Ya Zaitseva, I.S. Kovalyova, YuN. Mikhailov, Synthesis and crystal structure of $Cs_3ZnBr_5$, Russ. J. Inorg. Chem. 55 (2010) 1882–1887, https://doi.org/10.1134/S0036023610120119.
[15] A.I. Kruglik, A.D. Vasil'ev, G.V. Kovalev, Crystal structure of cesium cadmium bromide ($Cs_3CdBr_5$) and ammonium rubidium zinc bromide ($(NH_4)_{2.34}Rb_{0.66}ZnBr_5$), Kristallografiya 37 (1992) 583–588.
[16] B.N. Figgis, P.A. Reynolds, The crystal structure of tricaesium tetrabromocobaltate (II) bromide, $Cs_3CoBr_5$, at 4.2 K by neutron diffraction, Aust. J. Chem. 34 (1981) 2495–2498, https://doi.org/10.1071/CH9812495.
[17] H.P. Klug, L. Alexander, The crystal structure of ammonium pentachlorozincate, J. Am. Chem. Soc. 66 (1944) 1056–1064, https://doi.org/10.1021/ja01235a001.
[18] K. Friese, G. Madariaga, T. Breczewski, Tricaesium tetraiodozincate(II) iodide, $Cs_3ZnI_5$, Acta Crystallogr. C 54 (1998) 1737–1739, https://doi.org/10.1107/S0108270198008361.
[19] M. Heming, G. Lehmann, G. Henkel, B. Krebs, Correlation of zero field splittings and site distortions. III. $MnBr_4^{2-}$ and crystal structure refinements for $Rb_3ZnBr_5$ and $Cs_2ZnBr_4$, Z. Naturforschung 36A (1981) 286–293.
[20] W. Clegg, M.L. Brown, L.J.A. Wilson, Tricaesium tetrachloromercurate(II) chloride, Acta Crystallogr. B 32 (1976) 2905–2906, https://doi.org/10.1107/S0567740876009199.
[21] V.I. Pakhomov, P.M. Fedorov, G.G. Sadikov, Structure of cesium mercury bromide ($Cs_3HgBr_5$) crystals, Kristallografiya 23 (1978) 615–616.
[22] R. Sjövall, C. Svensson, Structure refinement of three caesium mercury iodides, $Cs_2Hg_3I_8.H_2O$, $Cs_2HgI_4$ and $Cs_3HgI_5$, Acta Crystallogr. C 44 (1988) 207–210, https://doi.org/10.1107/S0108270187009673.
[23] A. Kohne, E. Kemnitz, H. Mattausch, A. Simon, Crystal structure of caesium trichloroferrate(II), $CsFeCl_3$, Z. für Kristallogr. - Cryst. Mater. 203 (1993) 316–317, https://doi.org/10.1524/zkri.1993.203.Part-2.316.
[24] V.G. Meyer, Chlorometallate(III) mit Barytstruktur: $CsFeCl_4$ und $CsAlCl_4$, Z. Anorg. Allg. Chem. 436 (1977) 87–94, https://doi.org/10.1002/zaac.19774360109.
[25] V.H.-J. Seifert, K. Klatyk, Über die Systeme RbCl/$FeCl_2$ und CsCl/$FeCl_2$, Z. Anorg. Allg. Chem. 342 (1966) 1–9, https://doi.org/10.1002/zaac.19663420102.
[26] H. Yamatera, K. Nakatsu, The crystal structure of $Cs_3Fe_2Cl_9$ and of $Cs_3Sb_2Cl_9$, BCSJ 27 (1954) 244, https://doi.org/10.1246/bcsj.27.244.
[27] Agilent, CrysAlis PRO, Agilent Technologies Ltd, Yarnton, Oxfordshire, England, 2014, 2014.
[28] SCALE3 ABSPACK - an Oxford Diffraction Program (1.0.4,gui:1.0.3) (C), Oxford Diffraction Ltd., 2005.
[29] G.M. Sheldrick, Crystal structure refinement with *SHELXL*, Acta Crystallogr. C 71 (2015) 3–8, https://doi.org/10.1107/S2053229614024218.
[30] A.L. Spek, A.L. Spek, A Multipurpose Crystallographic Tool, Utrecht University, Utrecht, The Netherlands, 2014.
[31] G. Kortüm, Reflectance Spectroscopy, Springer, New York, 1969.
[32] W. Kohn, L.J. Sham, Self-consistent equations including exchange and correlation effects, Phys. Rev. A 140 (1965) 1133–1138, https://doi.org/10.1103/PhysRev.140.A1133.
[33] P.E. Blöchl, Projector augmented-wave method, Phys. Rev. B 50 (1994) 17953–17979, https://doi.org/10.1103/PhysRevB.50.17953.
[34] G. Kresse, D. Joubert, From ultrasoft pseudopotentials to the projector augmented-wave method, Phys. Rev. B 59 (1999) 1758–1775, https://doi.org/10.1103/PhysRevB.59.1758.
[35] G. Kresse, J. Furthmüller, Efficiency of ab-initio total energy calculations for metals and semiconductors using a plane-wave basis set, Comput. Mater. Sci. 6 (1996) 15–50, https://doi.org/10.1016/0927-0256(96)00008-0.
[36] J.P. Perdew, K. Burke, M. Ernzerhof, Generalized gradient approximation made simple, Phys. Rev. Lett. 77 (1996) 3865–3868, https://doi.org/10.1103/PhysRevLett.77.3865.
[37] R.D. Shannon, Revised effective ionic radii and systematic studies of interatomic distances in halides and chalcogenides, Acta Crystallogr. A 32 (1976) 751–767, https://doi.org/10.1107/S0567739476001551.
[38] R. Mason, E.D. McKenzie, G.B. Robertson, G.A. Rusholme, Thioacetylacetone complexes of iron(II), Chem. Commun. (London) (1968) 1673, https://doi.org/10.1039/c19680001673.
[39] J.W. Lauher, J.A. Ibers, Structure of tetramethylammonium tetrachloroferrate(II). Comparison of iron(II) and iron(III) bond lengths in high-spin tetrahedral environments, Inorg. Chem. 14 (1975) 348–352, https://doi.org/10.1021/ic50144a029.
[40] J. Goodyear, D.J. Kennedy, Crystal structure of $Cs_3MnCl_5$, Acta Crystallogr. B 32 (1976) 631–632, https://doi.org/10.1107/S0567740876003610.
[41] N.E. Brese, M. O'Keeffe, Bond-valence parameters for solids, Acta Crystallogr. B 47 (1991) 192–197, https://doi.org/10.1107/S0108768190011041.
[42] A. Altomare, C. Cuocci, C. Giacovazzo, A. Moliterni, R. Rizzi, N. Corriero, A. Falcicchio, *EXPO2013*: a kit of tools for phasing crystal structures from powder data, J. Appl. Crystallogr. 46 (2013) 1231–1235, https://doi.org/10.1107/S0021889813013113.